




# Inferring material parameters from imprecise experiments on soft materials by virtual fields method

N. Afsar Kazerooni<sup>1</sup> · Z. Wang<sup>2</sup> · A. R. Srinivasa<sup>1</sup>  · J. C. Criscione<sup>3</sup>

Received: 12 April 2020 / Accepted: 15 October 2020 / Published online: 4 November 2020  
© Springer-Verlag GmbH Germany, part of Springer Nature 2020

## Abstract

Inferring material parameters of soft materials, especially soft tissues from experiments, has always been a challenge because of the inaccuracy of specimen geometry, difficulty in proper gripping and difficulty in obtaining reliable displacement data. If one is able to obtain full field data with Digital Image Correlation or other similar techniques, we show that in spite of poor quality experimental data, it is still possible to get the material parameters using Virtual Fields Method with carefully chosen virtual fields. We demonstrate the approach by two cases. The first is Ecoflex (silicone rubber) under biaxial deformations at controlled loading rates, and the second is rat skin samples with imperfect shape under biaxial deformations at controlled loading rates. In both cases, rather than trying to obtain homogeneous deformation conditions, we use a technique based on the Virtual Fields Method to extract the material properties from the deformation of the specimen collected by Digital Image Correlation (DIC) and the force load measured by the load sensor. In order to apply loads in two principal directions simultaneously, a custom biaxial set-up was built and mounted into a uniaxial Instron tensile set-up. We show here that in spite of significant inhomogeneity in the deformation, errors, and missing data in the measured displacement field, we are still able to recover the material properties of the soft solid by suitable choices of virtual fields.

**Keywords** Skin · Silicone rubber · Biaxial cyclic tension testing · Digital image correlation · Heterogeneous deformation · Virtual field method · Material parameter estimation

## 1 Introduction

Stratified, epidermis, dermis, and newly discovered layer of fluid vesicles (called the interstitium) are the different layers of skin [4, 26]. Also, there is a fat layer under the dermis which separates the skin from muscles and other

organs. In order to find the mechanical properties of skin, it is necessary to study the behavior of all of these layers under mechanical loading. Since dermis is the major layer of skin that contains all collagen, elastic fibers, extrafibrillar matrix, hair follicles, etc., the mechanical properties of skin are usually defined by dermis [12]. The strength of the skin depends on fiber networks (especially collagen and elastin fibers in the epidermis). Due to the existence of these fibers, skin shows anisotropic behavior and shows different responses in different directions with respect to the spine.

Extracting material properties from experiments is essential problem for both engineers and researchers. Typically, the material properties are obtained from uniaxial tension tests based on the assumption of homogenous deformation. To investigate this behavior of skin, uniaxial tension testing was performed on samples with different orientation with respect to the spine [1–18], this approach is not very close to the condition found in vivo. Finding more similar situations to real life leads to measure the properties of orthotropic materials under biaxial tension tests. So, to better understand the mechanical behavior of soft tissues, it is essential

✉ A. R. Srinivasa  
asrinivasa@tamu.edu

N. Afsar Kazerooni  
nazanin26@tamu.edu

Z. Wang  
zhujiang.wang@hotmail.com

J. C. Criscione  
jccriscione@tamu.edu

<sup>1</sup> Department of Mechanical Engineering, Texas A&M University, College Station, TX 77843, USA

<sup>2</sup> Health Sciences, Ontario Tech University, 2000 Simcoe St N, Oshawa, ON L1G 0C5, Canada

<sup>3</sup> Department of Biomedical Engineering, Texas A&M University, College Station, TX 77843, USA

to run tests not only in uniaxial tension but in biaxial tension, which are widely used.

Many studies on biaxial testing of biological tissues exist, such as canine myocardium [36], arterial wall [37], pericardium [30], fresh valve [6], human myocardium [33], human skin [24], etc. There are a few studies on biaxial testing of skin, most of the studies on the skin are under uniaxial loading. The very first biaxial testing on the skin was performed by Lanir et al. [22, 23]. They tested rabbit skin under biaxial testing at different strain rates. They used video dimensional analyzers (VDA) to measure the distance between pairs of dark lines on the sample to find the amount of stretch. Flynn et al. [10] did biaxial tension testing on rat skin; their samples had a cross shape and connected to load cells, and they applied a load and removed it multiple times. Displacements were calculated by tracking markers movement. Capek et al. [8] built an *in vivo* biaxial device which is able to measure loads and displacement in two perpendicular directions by two load cells, and they only compared load-displacement curves in both directions.

Recently Digital Image Correlation (DIC) is heavily used to find the displacement field of soft tissue under stress. For example, [9] used DIC to find the mechanical properties of human skin. Later, [34] performed a bulge test on human skin using a custom pressure-controlled inflation system to investigate the effect of humidity and mechanical preconditioning. In their study, samples were cut from the back torso of the human body in a square shape, and then they were attached to a Plexiglas ring, and the displacement field was measured by DIC. In their method, it is difficult to find the stress and material parameters due to the curvature. Later, Maiti et al. [24] used a Correlated Solutions DIC system (Limes GmbH, Pforzheim, Germany) and Vic3D software to the flat part of the medial forearm [24].

Usually, in mechanical testing, to find material parameters, there is a relation between unknown parameters and measurements such as local deformation and applied loads. The assumptions in these cases are generally too strict; so for example, the assumption of uniform traction distribution on the sample close to grips.

Many times, especially for soft materials, experiments cannot be carried out with precision, for example, it may not be possible to grip the sample correctly, or specimen geometry is inaccurate, or the material is anisotropic and shows heterogeneous strain fields. So there's a need for other approaches based on the processing of heterogeneous strain fields. Due to all these issues, it may not be possible to get the full-field DIC measurements. However, given the fact that it should be possible to get a couple of constants even with poor fields.

One method to extract material parameters under the described conditions is Virtual Fields Method (VFM). This new technique, is based on the principle of virtual work (see

Sect. 4). It is crucial to develop virtual fields based on the observed deformation field. One of the early works in VFM was done by Grédiac et al. [13] on a T shape specimen to measure the stiffness of orthotropic materials directly. Later, Grédiac et al. [16, 17] used special virtual fields to extract material parameters for an in-plane case. Sometimes, data are noisy, and there is a need to extract material parameters. Grédiac et al. used numerical implementation of the VFM to extract material parameters after adding white noise to data [14]. In another work regarding noise in the data by [3], the sensitivity of the virtual field to noise was investigated. They proposed criteria for grading virtual fields and finding the sensitivity to noise. Later, Toussant et al. used a piece-wise virtual field to extract material parameters [35]. Recently, [25] used the sensitivity-based virtual fields for large deformation for anisotropic plasticity models.

In a few past years, this method has been used to extract material properties of soft tissues. Avril et al. [2] identified the material parameters of human arteries under finite inflation and extension and reported the anisotropic hyperelastic properties of the artery. They used the full-field data from experiments and showed that it is possible to get material parameters in Holzapfel model [19] and Fung model [11] by using different virtual fields.

One of the challenges in soft tissue is gathering full-field data from experiments. Usually, due to wrinkles or fluids in soft tissues, it is challenging to get very good speckle patterns, and it may not be possible to get the full-field data. The focus of this paper is to show that in spite of poor quality experimental data, it is still possible to get the material parameters. In the following sections, two cases are studied. The first case is Ecoflex samples (as a tissue simulator) are studied under biaxial deformations at controlled loading rates, and material parameters are obtained by VFM. The second one is skin samples (as an actual tissue) with imperfect shape are tested under biaxial deformations at controlled loading rates, and material parameters are obtained by VFM.

## 2 Materials and methods

### 2.1 Sample preparation for Ecoflex

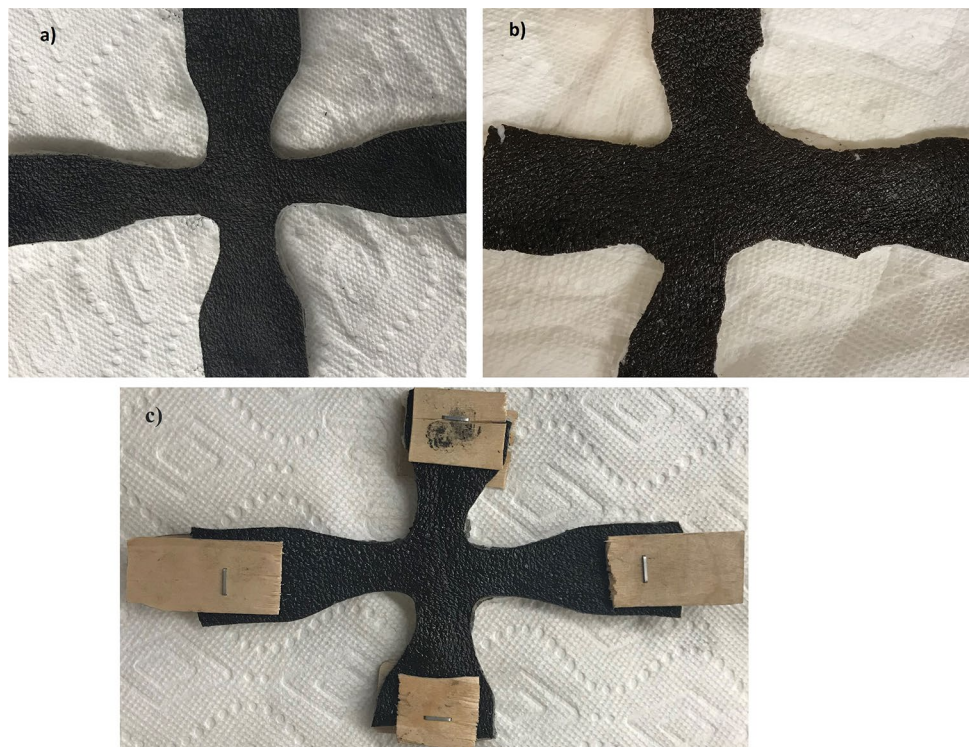
To do biaxial tension testing, samples were prepared from Ecoflex<sup>TM</sup> rubbers. They are platinum-catalyzed silicones made by mixing the same amount of part A and part B. The mixture will be cured after four hours. Then biaxial samples [31] were cut from the sheet with an average thickness of 3.5 mm. Then the mixture was poured in the mold to make a sheet. Since the strain field is obtained by Digital Image Correlation, after cutting samples, the pigment was sprayed by an electric toothbrush to get random speckles in speckle patterns. In order to prevent slipping

of samples out of the grips, Fig. 1 shows that small pieces of sandpaper were glued with super-glue on the surface of samples which are in contact with grips.



**Fig. 1** Ecoflex (silicone rubber) sample after preparation for biaxial testing

**Fig. 2** **a** Skin sample cut by Universal laser system, **b** Skin sample cut by scapula and **c** Skin sample after preparations



## 2.2 Sample preparation for skin

Skin samples from the abdominal and back region of an adult porcine were harvested at the Veterinary School of Texas A&M University. In order to apply a speckle pattern on the skin to study the deformation field, hair was removed from the skin using a razor blade. In all samples, the fat layer was removed, and epidermis and dermis were studied. Samples were cut by scapula firstly. Since pig skin is very tough, it was challenging to cut samples for biaxial testing, so a laser cutter was used to cut samples. Figure 2a, b show a sample cut by Universal Laser System versus a sample cut by scapula. In order to prevent slipping of samples from grips, pieces of wood were stapled on each side of a sample. Then the attached pieces of wood were gripped. The next step is preparing samples for Digital Image Correlation. Since the color of samples was dark gray, there is not enough contrast between speckles and background. Black pigment was applied on samples. Figure 2c shows a biaxial sample after preparation. To get a very random and uniform pattern, after gripping the sample, the white pigment was sprayed by an electric toothbrush on samples with black pigments (Fig. 3).

## 2.3 Biaxial set-up

A biaxial tension testing set-up has been devised, based on Brieu's design [7], to perform a more in-depth study of the mechanical behavior of skin and investigate the mechanisms



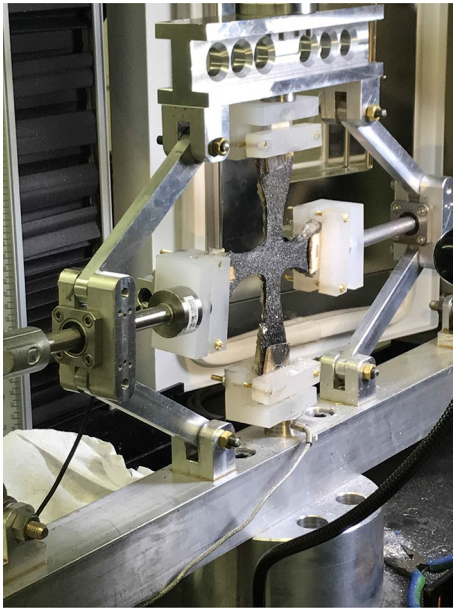
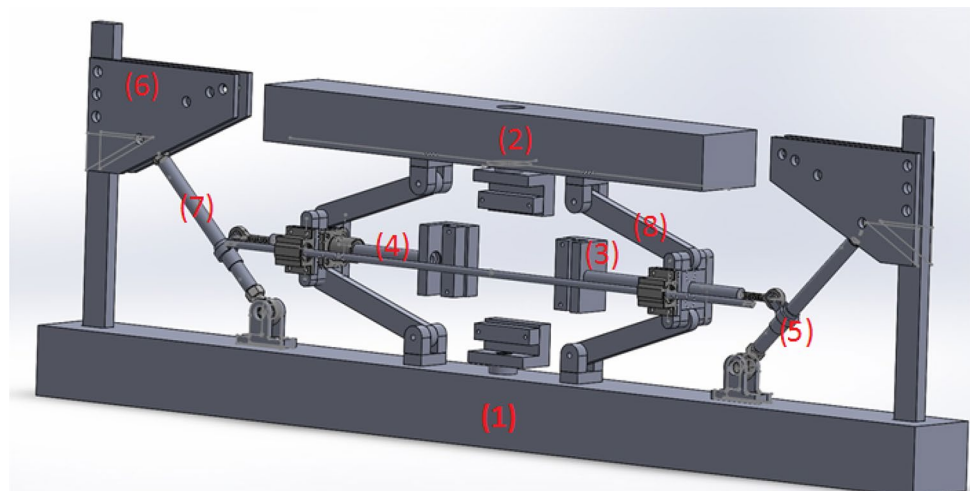


**Fig. 3** Skin sample is gripped in biaxial testing machine

of tearing of soft tissue. The main idea behind the designing of this new biaxial set-up is to build a low cost biaxial set-up which is adaptable to uniaxial tensile testing machines. Another advantage of this biaxial set-up is that it can be adjusted to be both equibiaxial and nonequibiaxial. Figure 4 shows the schematic design of the biaxial tensile test mechanism. Biaxial set-up is made of a few components that help stretching sample in two perpendicular directions, and these components are:

1. Fixed crosshead
2. Moving crosshead
3. Grip (2 grips in vertical direction and 2 grips in horizontal direction)

**Fig. 4** Schematic design of the biaxial tensile test mechanism



4. Horizontal sliding bar
5. Part for adjusting of the ratio of stretching between vertical and horizontal directions
6. Oblique Bar
7. Drawing plate
8. Sliding bearing

Part 1 is screwed to the bottom of the Instron machine, and it is fixed. Part 2 is connected to the top part of the Instron machine, which moves and part 2 can move with it. When part 2 is moving up by the movement of the Instron machine crosshead, the angle between drawing plates (part 8) increases and sliding bearings (part 5) are sliding on oblique bars (part 7). While sliding bearings are moving up, horizontal sliding bars are moving and pull both horizontal grips and lead to stretching the sample in the horizontal direction. Also, there is a stretch in the vertical direction due to the movement of the crosshead. One of the limitations of biaxial testing machines is that they are usually equibiaxial set-up. In this design, by changing the  $\phi$  angle, the angle between the oblique bar and the fixing crosshead (part 1), we can have both equibiaxial and nonequibiaxial set-up Fig. 4. In order to change this angle, the oblique bar can be connected to each hole in part 6. If the angle is 45 degrees, it shows equibiaxial behavior, and if  $\tan \phi$  is 2, 3 or 4, it is nonequibiaxial [7]. It is important to find a strain field and homogeneous region of deformation on a sample that is submitted to biaxial tensile testing. Digital Imaging Correlation (DIC) is useful and gives helpful information on the strain field and deformation in each direction. Since it is biaxial testing and the column of the Instron block the light on some part of the sample, another light source was used to get better contrast between the speckles and the background. Then the aperture and focus on each camera were adjusted based on the distance between the cameras and the sample. The next step is the system calibration to find internal system parameters and the relative position of the two cameras to each other. In order

to do the calibration, the calibration plate with a suitable size that covers the field of view of the cameras was chosen Fig. 7. After calibration, a set of images were captured every few seconds during the test. The correlations were based on images taken with the two video cameras that were analyzed by Istra 4D software (DANTEC DYNAMICS, Germany). From these sets of images, displacement and strain can be calculated from dots and their position during the deformation. Figure 5 shows the biaxial set-up, which is adaptable in a uniaxial machine and the DIC set-up. In order to measure loads in both horizontal and vertical directions, load-cells should be added to the set-up before grips in both directions (Fig. 6).

## 2.4 Experiments

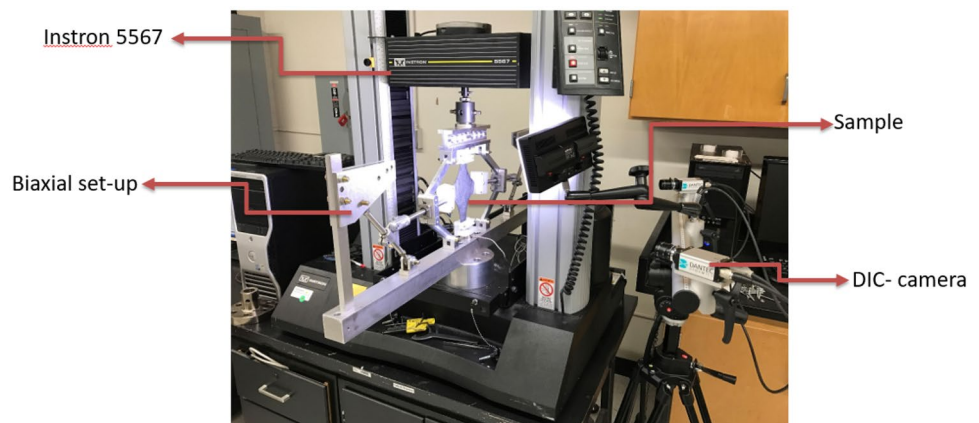
First, biaxial tension testing with an angle of 63.44 degrees was done on Ecoflex samples. During the test, samples at the strain rate of 0.5 mm/s were loaded to a specific elongation and then partially unloaded till reaching a certain

elongation and then repeated this loading and unloading cycles for few times at room temperature.

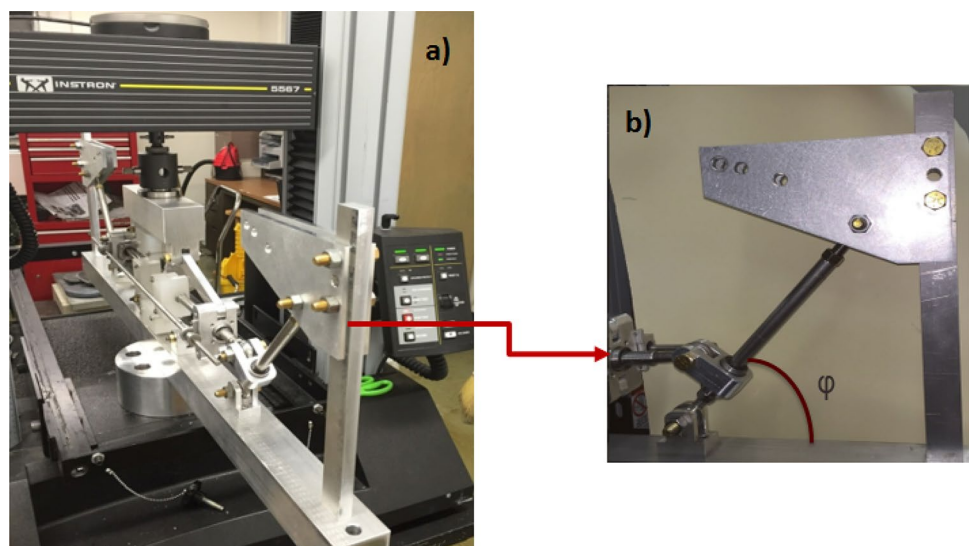
After testing Ecoflex, cyclic tension loading was done on skin samples. Skin samples were tested in the biaxial fixture with the  $\phi$  angle of 63.44°, and they were tested at room temperature and the strain rate of 10 mm/min. Firstly, samples were stretched to a specific elongation and then partially unloaded until reaching a certain elongation. In order to keep the samples wet during the tension tests and prevent them from drying and prevent the skin from changing so that it does not affect the behavior of skin [5], Veterinary 0.9 percent Sodium Chloride solution was sprayed on each sample during the test.

Then strain controlled loading and unloading cycles were repeated a few times, and the strain field was measured by Digital Imaging Correlation (DIC). The DIC system that was used is the Q-400 DIC system. The correlations are based on images taken with the two video cameras and processed using Istra 4D software.

**Fig. 5** Biaxial set-up on uniaxial tension machine (INSTRON 5567)



**Fig. 6** **a** Biaxial set-up, **b** Horizontal displacement, adjusted for equibiaxial and non-equibiaxial set-up



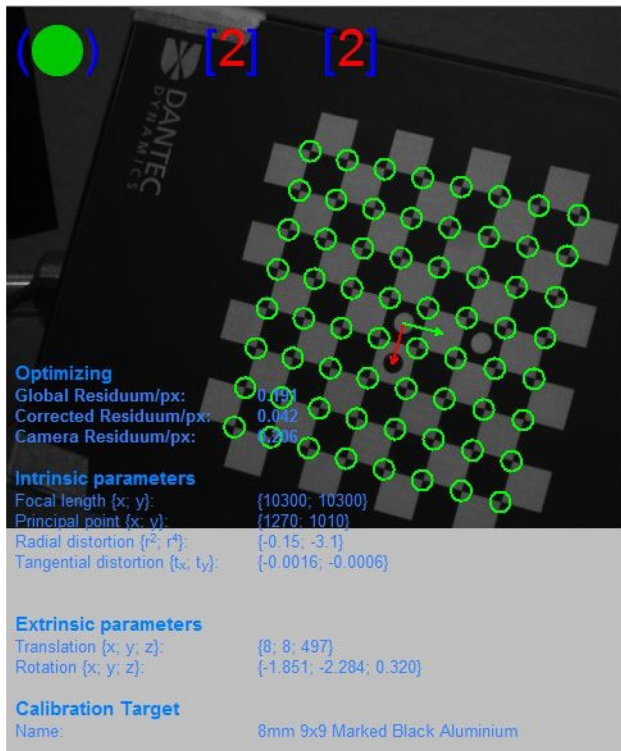


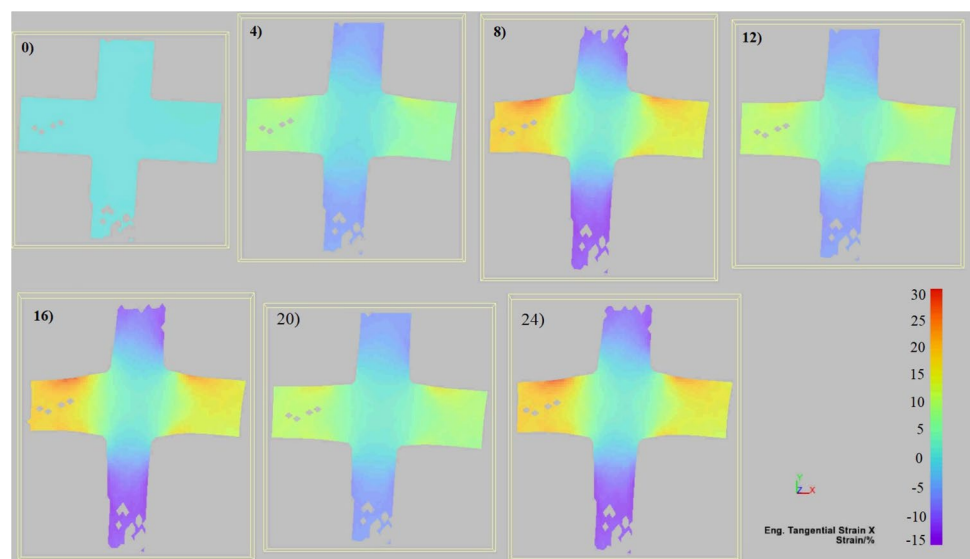
Fig. 7 Calibration plates are used to calibrate the system

## 3 Result and discussion

### 3.1 Ecoflex

Figures 8 and 9 show the engineering strain fields on the sample at different steps during the test. Each step is the deformation field that DIC image is taken during deformation. Loads in both vertical and horizontal direction under

Fig. 8 Engineering strain of Ecoflex sample in x-direction for each step during cyclic loading. Fewer data points are missing in Ecoflex compared to skin (Fig. 15)



biaxial cyclic loading are demonstrated in Fig. 10. As these two figures show, fewer data points are missing in engineering strain fields of Ecoflex compared to engineering strain fields of skin (Figs. 15 and 14). Also, they show that the deformation in the middle of the sample is more uniform and homogeneous in comparison with the deformation in skin (Figs. 15 and 14). Figure 11a and b show the grids on sample during biaxial testing, which were taken by DIC. It is evident that by improving the condition of the light on the sample and random speckle pattern with speckles with the uniform size, it is possible to get images with higher quality, which provide more information on the deformation field.

### 3.2 Skin

The next step is finding material parameters of skin under biaxial testing. After running biaxial testing, Istra 4D software is used to analyze images and create grids on samples. Each grid point defines the center of a squared image region in the reference image. These points are used in image correlation algorithm. Figure 12 shows grids on samples during biaxial testing, which were taken by DIC. These images show that the contrast between the background and speckle patterns is very important to get the maximum information from the speckle patterns. However, due to the existence of wrinkles and moisture on soft tissues, some parts of the deformation field are lost.

As it was discussed deformation field was measured by DIC during biaxial testing, and loads were measured by two different load cells in both horizontal and vertical direction, which are shown in Fig. 13 the load measurements from load cells in both vertical and horizontal directions. It was observed that after the first cycle, softening happened and there is a reduction in load after the first cycle at specific strain, which is called the Mullins effect. Figures 14 and 15 show the engineering strain fields on the sample and expresses the partial



**Fig. 9** Engineering strain of Ecoflex sample in y-direction for each step during cyclic loading. Fewer data points are missing in Ecoflex compared to skin (Fig. 14)

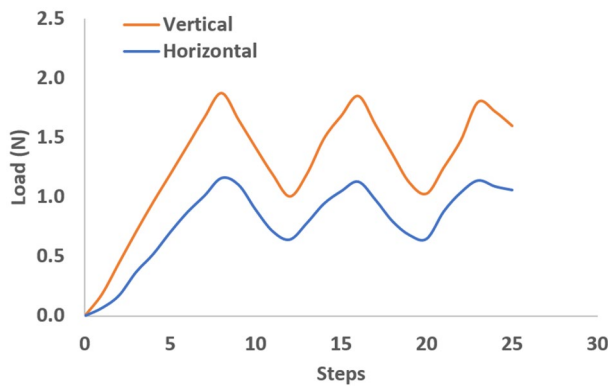
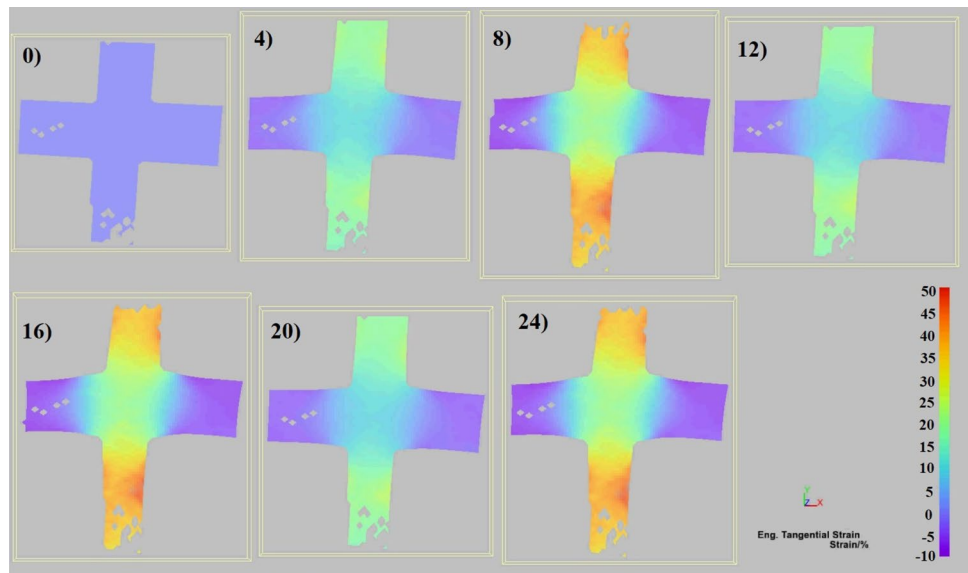


**Fig. 10** Loads in both horizontal and vertical directions for Ecoflex under biaxial testing under strain rate of 0.5 mm/s

strain fields. There are missing data points in strain fields in skin because of the nature of skin, which has wrinkles, and it is difficult to get the full strain field data in comparison with Ecoflex (Figs. 8, 9). Also, as Figs. 14 and 15 show the deformation is not homogeneous for skin. These are the preliminary results, but yet it is possible to extract the material parameters from these partial data by using the Virtual Fields Method (VFM). The two pieces of data, partial strain field through the body and forces of both directions, would be sufficient to extract the material properties.

## 4 Model and theory

### 4.1 Virtual fields method

As it was discussed earlier, VFM is based on the principle of virtual work [15].

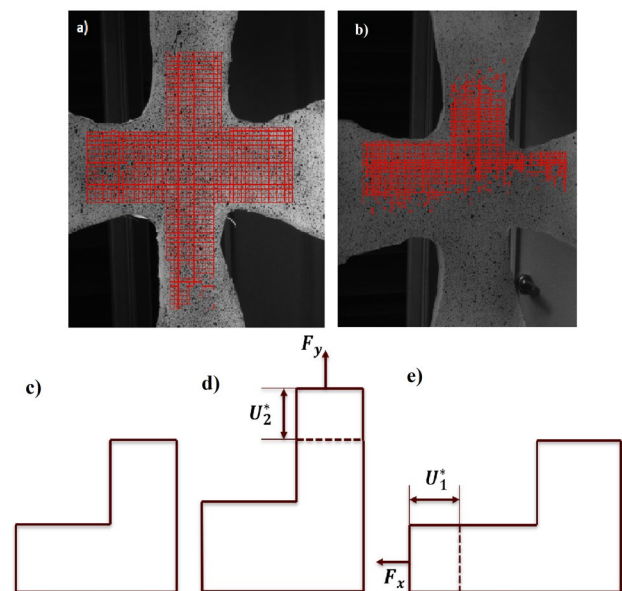


**Fig. 11** **a** High quality pattern; **b** low quality pattern. Despite all the severe imperfection in image (b), it is still possible to extract some material properties; **c** the deformation field we have chosen; **d** the first virtual field we create, where the virtual displacement in the vertical direction at the upper boundary is  $U_1^*$ . In this way, the virtual work done by external load is  $W_1^* = F_y * U_1^*$ ; **e** the second virtual field we create, where the virtual displacement in the horizontal direction at the left boundary is  $U_2^*$ . In this way, the virtual work done by external load is  $W_2^* = F_x * U_2^*$ .

$$\begin{aligned}
 & - \int_V \mathbf{FS} : \text{Grad}(\mathbf{U}^*) dV + \int_{\partial V} \mathbf{T} \cdot \mathbf{U}^* dS \\
 & + \int_V \mathbf{b} \cdot \mathbf{U}^* dV = \int_V \rho \mathbf{a} \cdot \mathbf{U}^* dV.
 \end{aligned} \tag{1}$$

**Fig. 12** Grids on skin samples during biaxial testing

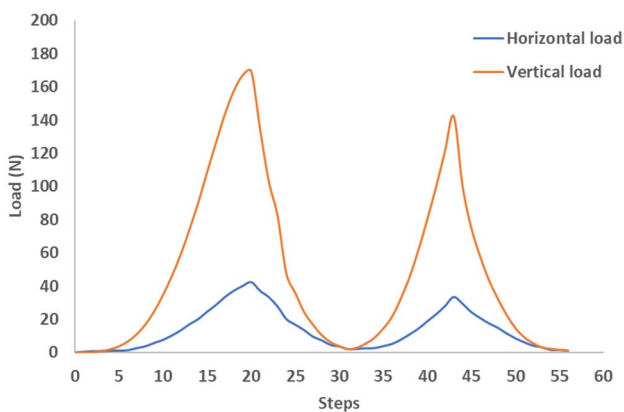
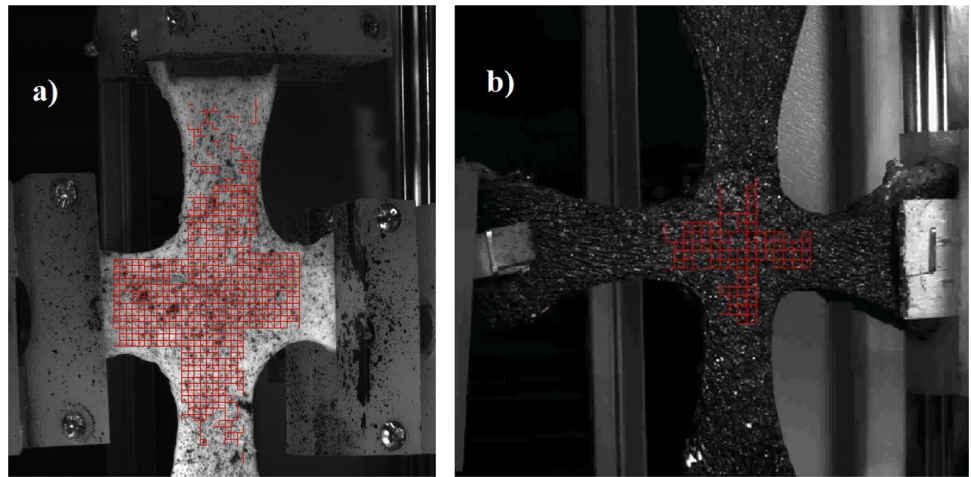


**Fig. 13** Loads in both horizontal and vertical directions during cyclic biaxial testing of rat skin at room temperature

where  $\mathbf{F}$  is the deformation gradient for the field we have chosen;  $\mathbf{S}$  is second Piola-Kirchhoff stress;  $\mathbf{T}$  is the traction vector on the boundary;  $\mathbf{U}^*$  any kinematic admissible virtual displacement field;  $\mathbf{b}$  body force;  $\mathbf{a}$  acceleration;  $\rho$  density.

We assume that there is no body force and there is a quasi-static loading process which leads to the elimination of two terms in Eq. 1 and the new equation is written as

$$\int_{\partial V} \mathbf{T} \cdot \mathbf{U}^* dS = \int_V \mathbf{FS} : \text{Grad}(\mathbf{U}^*) dV \quad (2)$$

In Eq. 1 the left side of the equation is the work done by internal forces and the right side of the equation is the work done by external forces.

Then with knowing the strain energy function, the external force, and choosing proper virtual fields, we can find

**Fig. 14** Engineering strain in y-direction for each step during cyclic loading. There are a lot of missing data points in the engineering strain field of skin in comparison with the engineering strain field of Ecoflex

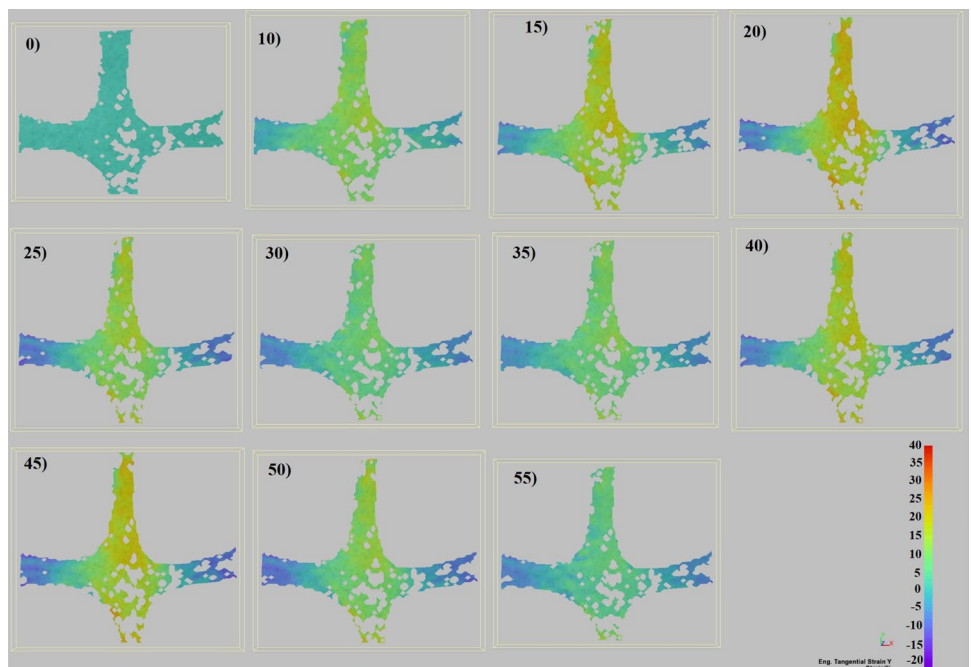
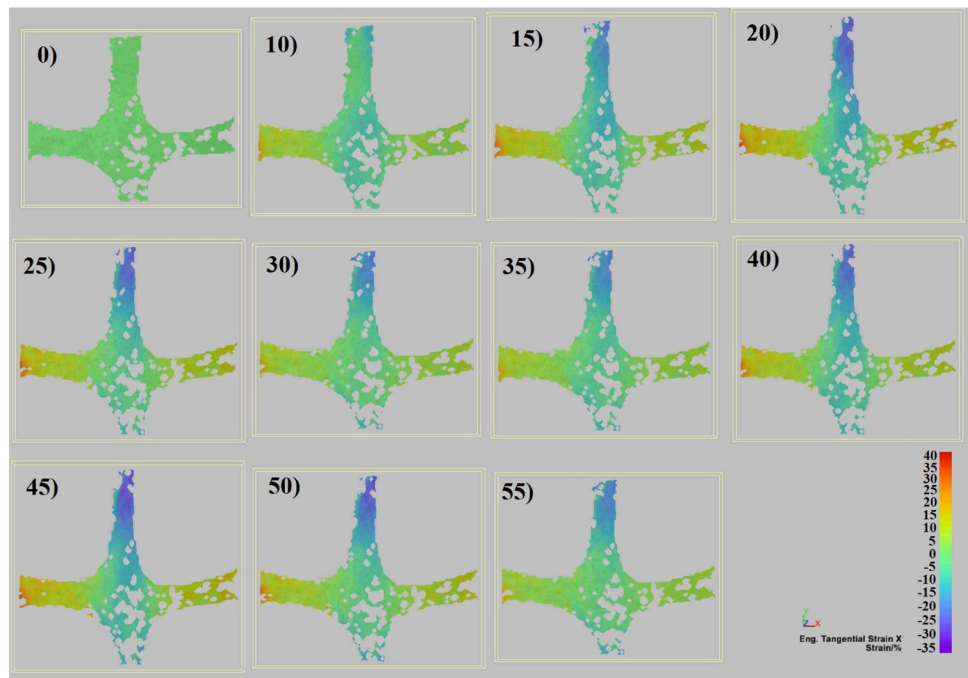




**Fig. 15** Engineering strain in x-direction for each step during cyclic loading. There are a lot of missing data points in the engineering strain field of skin in comparison with the engineering strain field of Ecoflex



the material parameters which we are going to show it for two cases Ecoflex and skin. The typical way to use the principle of virtual work is that the parameters are already known. Then the principle of virtual work is used to find the unknown displacements by choosing a proper test function. However, in the Virtual Fields Method, the actual displacement has been known from the DIC, and there is a need to find the unknown parameters by choosing a proper test function [15]. Figure 16 shows the summary of obtaining material parameters with the help of VFM. As it shows, after running experiments and assuming virtual fields, the principle of virtual work is used to get equations for the unknown parameters by knowing the constitutive equation with  $n$  parameters. Next step is choosing  $m$  virtual fields ( $m \geq n$ ). Then after finding the internal virtual work (IVW) based on the strain energy function and external virtual work (EVW) based on the external force, the error between them is obtained by using a proper cost function. In the end, material parameters are obtained by minimizing the cost function.

First, the Virtual Fields Method is used to find material parameters for Ecoflex, and then it is used to find material parameters for skin under biaxial testing.

### 4.2 Ecoflex

The Mooney-Rivlin model was used [27] and [29] for isotropic hyperelastic materials. Silicone rubber is assumed to be hyperelastic and incompressible [32]. Since the rate of stiffening is low for these materials with respect to soft tissues, which has a higher stiffening rate, it is common to

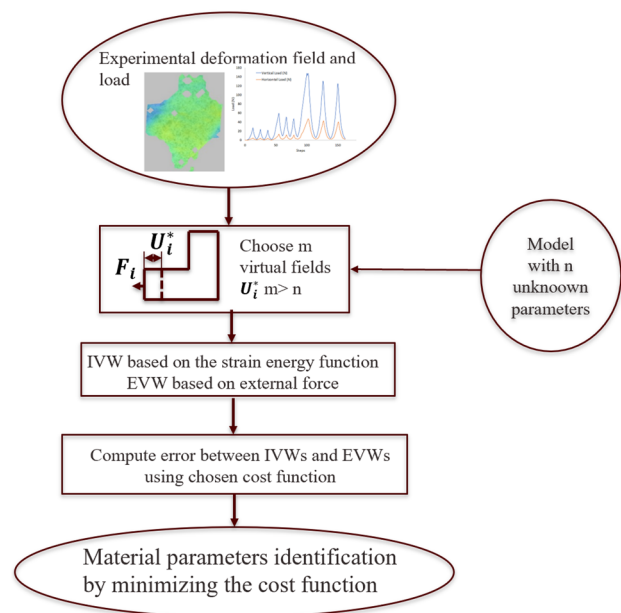


**Fig. 16** Diagram for implementation of VFM to find the material parameters. IVW is the internal virtual work and EVW is the virtual work done by external force

use the Mooney-Rivlin model to find its materials parameters [32]. So the strain energy function is

$$\Psi = [\mu_1(I_1 - 3) + \mu_2(I_2 - 3)]/2 \tag{3}$$

which is linear in parameters, where  $I_1$  and  $I_2$  are the first invariants and second invariants of the right Cauchy-Green

strain tensor  $\mathbf{C}$ . The second Piola-Kirchhoff stress is calculated as

$$\mathbf{S} = 2 \frac{\partial \Psi}{\partial \mathbf{C}} - p \mathbf{C}^{-1} = 2 \sum_{a=1}^2 \frac{\partial \Psi}{\partial I_a} \frac{\partial I_a}{\partial \mathbf{C}} - p \mathbf{C}^{-1}. \quad (4)$$

Since it is a membrane,  $p$  is eliminated. The parameters  $\mu_1$  and  $\mu_2$  need to be estimated from measurements.

In order to find material parameters  $\mu_1$  and  $\mu_2$ , Virtual Fields Method is used. Assuming that the deformation of the Ecoflex™ sample is quasi-statistic and there is no body force, we can obtain the following equation based on the principle of Virtual Fields Method (VFM) [15] for partial measured field:

$$\int_{\partial V} \mathbf{T} \cdot \mathbf{U}^* dS = \int_V \mathbf{F} \mathbf{S} : \text{Grad}(\mathbf{U}^*) dV. \quad (5)$$

where  $\mathbf{T}$  is the traction vector on the boundary;  $\mathbf{F}$  the deformation gradient for the field we have chosen;  $\mathbf{U}^*$  any kinematic admissible virtual displacement field; the left-hand side is the virtual work done by external loads; the right-hand side is the virtual work done by internal stresses. Figure 17 shows the virtual displacement for boundaries and inside the boundaries.  $x_i$  and  $y_i$  are the positions of the nodes of the grid in the deformed configuration. The virtual displacement for the bottom boundary points are zero, when  $x_i = x_b$ , we have  $(x_i^*, y_i^*) = (x_i, y_i)$  and after doing curve fitting for the bottom boundary points we have  $\bar{y} = f_b(x)$  so that  $f_b(x_b) = y_b$  where  $(x_b, y_b)$  are the coordinates of the points at the bottom boundary. In order to do curve fitting for the top boundary points we have  $\bar{y} = f_t(x)$  so that  $f_t(x_t) = y_t$ , where  $(x_t, y_t)$  are the coordinates at boundary points. Finally, the virtual displacement for the top boundary points is a constant  $U^*$ , where  $(x_i^*, y_i^*) = (x_i, y_i + U^*)$ . So, virtual fields are  $x_i^* = x_i$  and  $y_i^* = y_i + U^* \cdot \frac{y_i - f_b(x_i)}{f_t(x_i) - f_b(x_i)}$ .

Now assume for each virtual field of  $x_i^*$  we have

$$\int \delta \psi_i dV = \delta W(x_i^*) \quad (6)$$

Then let  $a_1(x_i^*) = 1/2 \int \delta I_1 dV$  and  $a_2(x_i^*) = 1/2 \int \delta I_2 dV$ , for  $i = 1, 2, \dots, 2 * N$

$$a_1(x_i^*) \mu_1 + a_2(x_i^*) \mu_2 = \delta W_i \quad (7)$$

$$\text{Let } \mathbf{A}(x^*) = [a_1(x_1^*), a_2(x_1^*); a_1(x_2^*), a_2(x_2^*); \dots, a_1(x_{2N}^*), a_2(x_{2N}^*)]$$

$$\mathbf{y} = [\delta W_1, \delta W_2, \dots, \delta W_{2N}]^T \quad (8)$$

Let  $\beta = [\mu_1, \mu_2]^T$ , then we can use linear least squares (Eq. 9) to find the material parameters which are  $\bar{\mu}_1$  and  $\bar{\mu}_2$  in Fig. 18.

$$\beta = (\mathbf{A}^T \mathbf{A})^{-1} \mathbf{A}^T \mathbf{y} \quad (9)$$

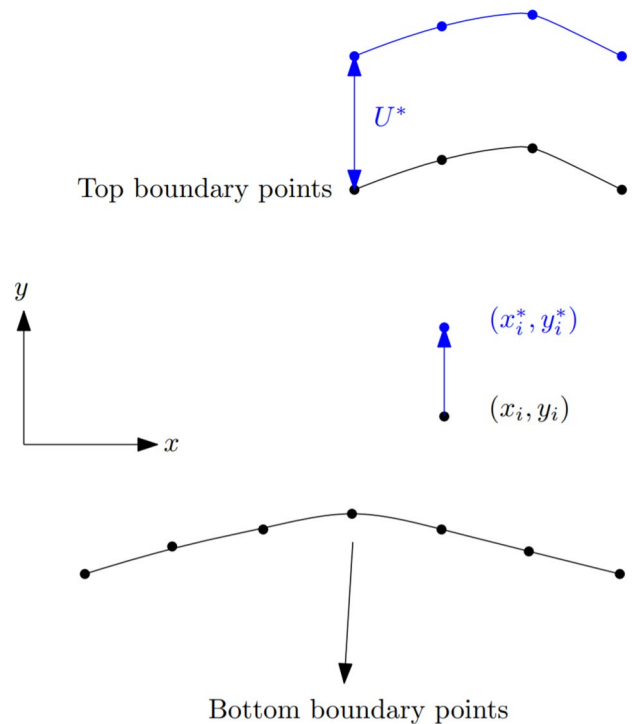


**Fig. 17** The virtual displacement for boundaries and inside the boundaries.  $x_i$  and  $y_i$  are the positions of the nodes of the grid in the deformed configuration

In order to find these material parameters, we can assign two virtual fields for the above equation, and therefore obtain two equations with two unknowns  $\mu_1$  and  $\mu_2$ . In the experiments, we measured seven different deformation fields; for each measurement, we assign two virtual fields, so there are a total of 14 equations and 2 unknowns. We assume that the noise in the measurements follows a Gaussian distribution; and then by employing the least squares method, we obtain the results shown in Fig. 18.  $\mu_1$  and  $\mu_2$  are the material properties obtained from each deformation step.  $\bar{\mu}_1 = 4.2$  MPa and  $\bar{\mu}_2 = 0.2$  MPa are the material properties obtained through the least square method for all the deformation measurements which are in the same ranges with the material parameters for these materials in the literature [32]. There are higher errors for lower deformations due to the slack in the machines and other imperfections in the set-up.

### 4.3 Skin

In this part, the well-known Holzapfel model is used for skin [19]. Assumptions in this work is that skin is incompressible, anisotropic. Also, Kazerooni et al. ([20]) showed that under cyclic loading, during the unloading part, skin shows elastic behavior. So, in this work, we only consider the unloading parts, which leads to another assumption that skin is elastic.

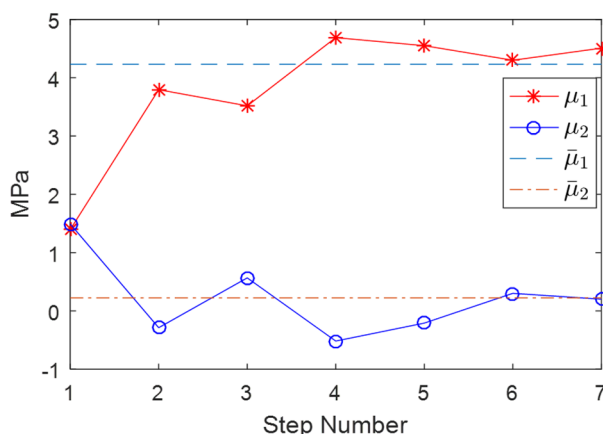


**Fig. 18**  $\mu_1$  and  $\mu_2$  are the material properties obtained from each deformation step (each deformation field is each image taken by DIC during deformation).  $\bar{\mu}_1$  and  $\bar{\mu}_2$  are the material properties obtained through the least square method for all the deformation measurements

$$\bar{\Psi} = \frac{C}{2} (\bar{I}_1 - 3) + \frac{k_1}{2k_2} \left[ e^{k_2(\bar{I}_4 - 1)} - 1 \right] + \frac{k_3}{2k_4} \left[ e^{k_4(\bar{I}_6 - 1)} - 1 \right] \tag{10}$$

In Eq. 10  $C$  is a parameter of isotropic non-collagenous materials and  $k_1, k_2, k_3$  and  $k_4$  are parameters to describe the anisotropic behavior of collagenous materials.  $\bar{I}_1$  is the first invariant of the right cauchy stress tensor and  $\bar{I}_4$  and  $\bar{I}_6$  are invariants to characterize the deformation of the two families of collagen fibers.

From the histology results, [1] major orientations of fibers are obtained by analyzing histology images. Figure 19 shows the schematic reference configuration of fibers orientations. Histology analysis shows that in Fig. 19  $\Phi_1$  is  $34^\circ$  and  $\Phi_2$  is  $-56^\circ$ . In this work, we use fiber orientations from histology and use it in the Holzapfel model, which is the most comfortable model that would accommodate this information and has a nice set-up with an isotropic background and fibers [19]. In Eq. 10  $C$  is a parameter of isotropic non-collagenous materials and  $k_1, k_2, k_3$  and  $k_4$  are parameters to describe the anisotropic behavior of collagenous materials. Usually, angles between fibers are not  $90^\circ$ , so for orthotropic materials, they assume that  $k_1 = k_3, k_2 = k_4$ . However, in our case, since the angle between the two major fibers directions is  $90^\circ$ , there is no need to have the above assumption, and all of the parameters exist.

Based on the principle of VFM ([15]), two different virtual fields were created. One of them is  $x_1^* = [x_v^*, y, z]$  and the other one is  $x_2^* = [x, y_v^*, z]$ .

Assume that the body force is neglected, and the loading process is quasi-static, for each virtual field (similar to Fig. 17 for Ecoflex)  $x_i^*$ , we have

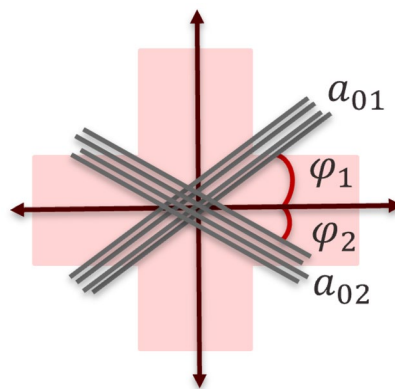


**Fig. 19** Reference configuration fibers orientation in two directions with the unit vectors of  $a_{01}$  and  $a_{02}$

$$\int_V \mathbf{P} : \delta \mathbf{F}_i = \delta W(\mathbf{x}_i^*) \tag{11}$$

where  $\mathbf{P} = \frac{\partial \Psi}{\partial \mathbf{F}}$  is the first Piola-Kirchhoff stress tensor, which can be expressed as  $\mathbf{P} = f(C, k_1, k_2, k_3, k_4)$  given the deformation field  $\mathbf{x}$ ;  $\delta \mathbf{F}_i = \frac{\partial(\mathbf{x}_i^* - \mathbf{x}_i)}{\partial \mathbf{X}}$ ;  $\delta W(\mathbf{x}_i^*)$  is the virtual work done by the external load.

Let  $\beta = [C, k_1, k_2, k_3, k_4]$ ,  $f_i = \int_V \delta \psi_i dV$ ,  $y_i = \delta W_i$  and assume we have  $N$  deformation field (load steps), then we have  $2N$  virtual fields and thus

$$f(x_i^*, \beta) = y_i, \quad i = 1 \dots 2N \tag{12}$$

We can use Levenberg–Marquardt algorithm to obtain the material constant  $\beta$  of Holzapfel model, which are shown in Table 1 and they are in the same ranges with the literature for soft tissues [28].

We can use the same method to obtain the material constant of Holzapfel model [19]. The virtual displacement for boundaries and inside the boundaries Based on VFM, we can obtain

$$\int_{\partial V} T \cdot U^* dS = \int_V FS : Grad(U^*) dV \tag{13}$$

where  $T$  is the traction vector on the boundary;  $F$  the deformation gradient for the field we have chosen;  $U^*$  any kinematic admissible virtual displacement field; the left-hand side is the virtual work done by external loads; the right-hand side is the virtual work done by internal stress.

$U_1^*$  is the virtual displacement in the vertical direction at the upper boundary, and  $W_1^* = F_y * U_1^*$  is the virtual work done by a vertical external load. Also,  $U_2^*$  is the virtual displacement in the horizontal direction at the left boundary, and the virtual work done by the horizontal external load is  $W_2^* = F_x * U_2^*$ .



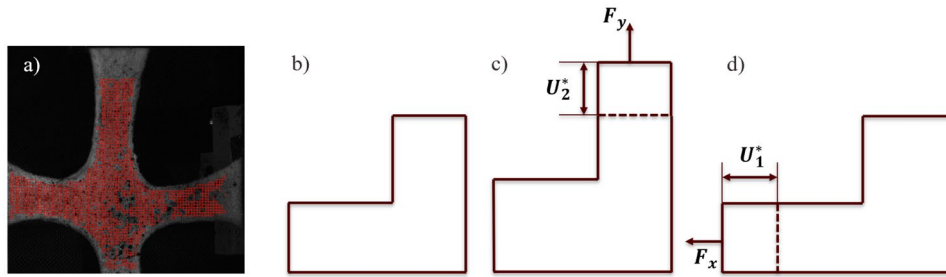


**Fig. 20** **a** DIC grid on rat sample with a pattern. Despite all the imperfection in image (**a**), it is still possible to extract some material properties; **b** the deformation field we have chosen; **c** the first virtual field we create, where the virtual displacement in the vertical direction at the upper boundary is  $U_1^*$ . In this way, the virtual work done by

external load is  $W_1^* = F_y * U_1^*$ ; **d** the second virtual field we create, where the virtual displacement in the horizontal direction at the left boundary is  $U_2^*$ . In this way, the virtual work done by external load is  $W_2^* = F_x * U_2^*$

**Fig. 21** When  $C, k_1, k_2, k_3$  and  $k_4$  are the material parameters: **a** Comparison between the internal virtual work 1 and the external virtual work 1, **b** Comparison between the internal virtual work 2 and the external virtual work 2 and **c** Comparison between the square differences of between internal virtual work and the external virtual work for both virtual field 1 and 2

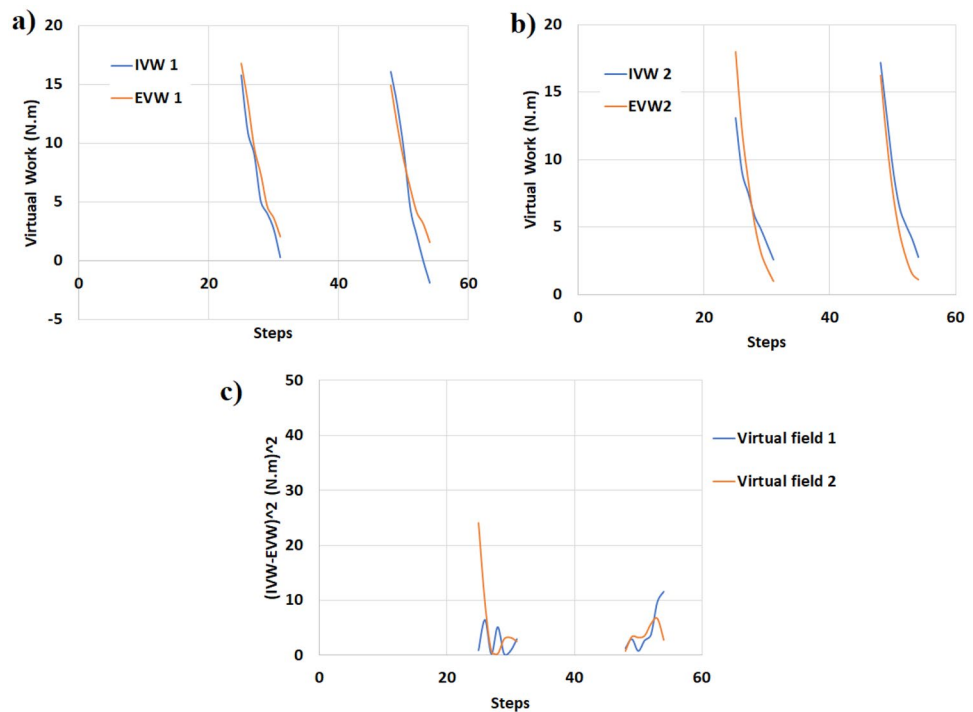


**Table 1** Table of parameters for skin based on Holzapfel model

Material parameters	$C$ (MPa)	$k_1$ (MPa)	$k_2$	$k_3$ (MPa)	$k_4$
Rat Skin	0.47	1.8	100	0.061	100

We used internal virtual work and the external virtual work at each step to identify material parameters. Now, the comparison between the internal virtual work and the external virtual work at each step shows whether it is a proper identification with VFM or not [21] (Fig. 20).

Figure 21 shows the comparison between the internal virtual work and the external virtual work at each step. In Fig. 21a, virtual works for virtual field 1 are shown, and in

Fig. 21b, virtual works for virtual field 2 are shown. Figure 21c shows the square difference between virtual works for each virtual field. As Fig. 21 shows, there is a good match between internal and external virtual works, which indicates there is a proper identification with VFM [21].

### 5 Conclusions

According to this study, behaviors of skin and Ecoflex were studied under biaxial cyclic loading test. We showed that in spite of poor quality experimental data, it is still possible to get the material parameters by choosing proper virtual fields.

With the help of VFM and full-field measurement technique, material parameters were extracted first for rubber ( $\mu_1$  and  $\mu_2$ ) and then for skin ( $C$ ,  $k_1$ ,  $k_2$ ,  $k_3$  and  $k_4$ ), despite the missing pieces of data and the heterogeneity in the strain field. However, these material parameters,  $k_1$ ,  $k_2$ ,  $k_3$  and  $k_4$  do not have a physical meaning. So it would be nice if they have a physical meaning, for example, based on a slope of the curve, which is the motivation for future studies.

**Acknowledgements** The authors gratefully thank Dr. Terry Creasy for allowing us to use his facilities and Dr. Goenezen for lending us, the DIC set-up.

## References

- Afsar-Kazerooni N, Srinivasa A, Criscione J (2020) Experimental investigation of the inelastic response of pig and rat skin under uniaxial cyclic mechanical loading. *Exp Mech* pp. 1–17
- Avril S, Badel P, Duprey A (2010) Anisotropic and hyperelastic identification of in vitro human arteries from full-field optical measurements. *J Biomech* 43(15):2978–2985
- Avril S, Grédiac M, Pierron F (2004) Sensitivity of the virtual fields method to noisy data. *Comput Mech* 34(6):439–452
- Benias PC, Wells RG, Sackey-Aboagye B, Klavan H, Reidy J, Buonocore D, Miranda M, Kornacki S, Wayne M, Carr-Locke DL et al (2018) Structure and distribution of an unrecognized interstitium in human tissues. *Sci Rep* 8(1):4947
- Berardesca E, Elsner P, Wilhelm KP, Maibach HI (1995) Bioengineering of the skin: methods and instrumentation, vol 3. CRC Press, Boca Raton
- Billiar KL, Sacks MS (2000) Biaxial mechanical properties of the natural and glutaraldehyde treated aortic valve cusp-part i: experimental results. *J Biomech Eng* 122(1):23–30
- Brieu M, Diani J, Bhatnagar N (2006) A new biaxial tension test fixture for uniaxial testing machine—a validation for hyperelastic behavior of rubber-like materials. *J Test Eval* 35(4):1–9
- Capek L, Lochman Z, Dzan L, Jacquet E (2010) Biaxial extensometer for measuring of the human skin anisotropy in vivo. In: 2010 5th Cairo International Biomedical Engineering Conference, pp. 83–85. <https://doi.org/10.1109/CIBEC.2010.5716059>
- Evans SL, Holt CA (2009) Measuring the mechanical properties of human skin in vivo using digital image correlation and finite element modelling. *J Strain Anal Eng Design* 44(5):337–345. <https://doi.org/10.1243/03093247JSA488>
- Flynn D, Peura G, Grigg P, Hoffman A (1998) A finite element based method to determine the properties of planar soft tissue. *J Biomech Eng* 120(2):202–210
- Fung YC (2013) *Biomechanics: mechanical properties of living tissues*. Springer Science & Business Media, Berlin
- Geerligs M (2006) In vitro mechanical characterization of human skin layers: stratum corneum, epidermis and hypodermis. Ph.D. thesis, Ph. D. Thesis, Technische Universiteit Eindhoven
- Grédiac M, Pierron F (1998) At-shaped specimen for the direct characterization of orthotropic materials. *Int J Numer Methods Eng* 41(2):293–309
- Grédiac M, Pierron F (2004) Numerical issues in the virtual fields method. *Int J Numer Methods Eng* 59(10):1287–1312
- Grédiac M, Pierron F, Avril S, Toussaint E (2006) The virtual fields method for extracting constitutive parameters from full-field measurements: a review. *Strain* 42(4):233–253
- Grédiac M, Toussaint E, Pierron F (2002) Special virtual fields for the direct determination of material parameters with the virtual fields method. 1—principle and definition. *Int J Solids Struct* 39(10):2691–2705
- Grédiac M, Toussaint E, Pierron F (2002) Special virtual fields for the direct determination of material parameters with the virtual fields method. 2—application to in-plane properties. *Int J Solids Struct* 39(10):2707–2730
- Haut R (1989) The effects of orientation and location on the strength of dorsal rat skin in high and low speed tensile failure experiments. *J Biomech Eng* 111(2):136–140
- Holzappel GA, Gasser TC, Ogden RW (2000) A new constitutive framework for arterial wall mechanics and a comparative study of material models. *J Elast Phys Sci Solids* 61(1):1–48
- Kazerooni NA, Srinivasa A, Freed A (2019) Orthotropic-equivalent strain measures and their application to the elastic response of porcine skin. *Mech Res Commun* 101:103404
- Kim JH, Avril S, Duprey A, Favre JP (2012) Experimental characterization of rupture in human aortic aneurysms using a full-field measurement technique. *Biomech Model Mechanobiol* 11(6):841–853
- Lanir Y, Fung Y (1974) Two-dimensional mechanical properties of rabbit skin—i. experimental system. *J Biomech* 7(1):29–34
- Lanir Y, Fung Y (1974) Two-dimensional mechanical properties of rabbit skin—ii. experimental results. *J Biomech* 7(2):171–182. [https://doi.org/10.1016/0021-9290\(74\)90058-X](https://doi.org/10.1016/0021-9290(74)90058-X)
- Maiti R, Gerhardt LC, Lee ZS, Byers RA, Woods D, Sanz-Herrera JA, Franklin SE, Lewis R, Matcher SJ, Carré MJ (2016) In vivo measurement of skin surface strain and sub-surface layer deformation induced by natural tissue stretching. *J Mech Behav Biomed Mater* 62:556–569
- Marek A, Davis FM, Rossi M, Pierron F (2018) Extension of the sensitivity-based virtual fields to large deformation anisotropic plasticity. *Int J Mater Form*. <https://doi.org/10.1007/s1228-9-018-1428-1>
- McGrath JA, Uitto J (2010) *Anatomy and Organization of Human Skin*, Chap. 3, pp. 1–53. Wiley-Blackwell. <https://doi.org/10.1002/9781444317633.ch3>
- Mooney M (1940) A theory of large elastic deformation. *J Appl Phys* 11(9):582–592
- Nolan D, Gower A, Destrade M, Ogden R, McGarry J (2014) A robust anisotropic hyperelastic formulation for the modelling of soft tissue. *J Mech Behav Biomed Mater* 39:48–60. <https://doi.org/10.1016/j.jmbbm.2014.06.016>
- Rivlin RS (1948) Large elastic deformations of isotropic materials. iv. further developments of the general theory. *Philos Trans R Soc Lond A: Math, Phys Eng Sci* 241(835): 379–397. <https://doi.org/10.1098/rsta.1948.0024>. <http://rsta.royalsocietypublishing.org/content/241/835/379>
- Sacks MS (2000) Biaxial mechanical evaluation of planar biological materials. *J Elast Phys Sci Solids* 61(1):199. <https://doi.org/10.1023/A:1010917028671>
- Seibert H, Scheffer T, Diebels S (2014) Biaxial testing of elastomers—experimental setup, measurement and experimental optimization of specimen’s shape. *Tech Mech* 34(2):72–89
- Shergold OA, Fleck NA, Radford D (2006) The uniaxial stress versus strain response of pig skin and silicone rubber at low and high strain rates. *Int J Impact Eng* 32(9):1384–1402. <https://doi.org/10.1016/j.ijimpeng.2004.11.010>. <http://www.sciencedirect.com/science/article/pii/S0734743X04002325>
- Sommer G, Haspinger DC, Andrä M, Sacherer M, Viertler C, Regitnig P, Holzappel GA (2015) Quantification of shear deformations and corresponding stresses in the biaxially tested human myocardium. *Ann Biomed Eng* 43(10):2334–2348. <https://doi.org/10.1007/s10439-015-1281-z>

34. Tonge TK, Atlan LS, Voo LM, Nguyen TD (2013) Full-field bulge test for planar anisotropic tissues: Part i-experimental methods applied to human skin tissue. *Acta Biomater* 9(4):5913–5925. <https://doi.org/10.1016/j.actbio.2012.11.035>
35. Toussaint E, Grédiac M, Pierron F (2006) The virtual fields method with piecewise virtual fields. *Int J Mech Sci* 48(3):256–264
36. Yin FC, Strumpf RK, Chew PH, Zeger SL (1987) Quantification of the mechanical properties of noncontracting canine myocardium under simultaneous biaxial loading. *J Biomech* 20(6):577–589
37. Zemánek M, Burša J, Děták M (2009) Biaxial tension tests with soft tissues of arterial wall. *Eng Mech* 16(1):3–11

**Publisher's Note** Springer Nature remains neutral with regard to jurisdictional claims in published maps and institutional affiliations.